Transactions of the Materials Research Society of Japan 29[7] 3103-3106 (2004)

γ'-Fe_4N Thin Films with Out-of-plane Magnetization

Kaoru Higashi and Katsuro Oda
Institute of Industrial Science, University of Tokyo, 4-6-1 Komaba Meguro-ku, Tokyo 153-8505, JAPAN
Fax: 81-3-5452-6326, e-mail: east@iis.u-tokyo.ac.jp

Highly oriented γ'-Fe_4N(001) films on MgO(001) and $SrTiO_3$(001) substrates and γ'-Fe_4N(111) films on MgO(111) and $SrTiO_3$(111) substrates were successfully grown by means of reactive sputtering. Due to the structural and magnetic measurements, γ'-Fe_4N(111) films show an out-of-plane magnetic anisotropy and the direction of magnetization in the films depends on their substrates.

Key words: γ'-Fe_4N, thin film, reactive sputtering, conversion electron Mössbauer spectroscopy, magnetic anisotropy

1. INTRODUCTION

We are aiming to develop toxic-free magnetic devices. From such point of view, iron nitrides are very attractive material. They are made up of very common elements and both elements in themselves are not harmful to the environment. The nitrides have large corrosion and wear resistance, and moreover, some of these have excellent magnetic properties. Therefore, potential application for high-density magnetic storage devices is expected [1].

γ'-Fe_4N is the most stable iron nitride phase, and is a ferromagnet which has large saturation magnetization (190emu/g) and the Curie temperature of 785K [2]. It adopts the cubic perovskite structure (a=3.795Å) with N atom located at the body-center of an fcc-Fe lattice. A Mössbauer spectrum of γ'-Fe_4N consists of three sextets which indicate ferromagnetic Fe atoms in one edge site and two magetically different face-center sites [3]. The easy axis of magnetization for γ'-Fe_4N is along <100> in both bulk and thin-film forms [3, 4].

Recently, epitaxial multilayers have attracted much attention with respect to magnetic devices like spin valve [5] and ferromagnetic tunnel junction [6]. In this study, we fabricated iron nitride films to obtain highly oriented γ'-Fe_4N for application to such devices, and investigated structural and magnetic properties of the films.

2. EXPERIMENTAL

Iron nitride thin films were fabricated by reactive RF magnetron sputtering using N_2. The base pressure in the deposition chamber was approximately 5×10^{-6} Pa. A RF magnetron sputter cathode and a N_2 gas inlet are located at angles of 60° and 30° to the surface of a substrate mounted on a rotating sample stage, respectively. The distance between the sputtering target and the substrate was 150mm.

We investigated hyperfine structure of γ'-Fe_4N films by conversion electron Mössbauer spectroscopy (CEMS). To acquire high signal/noise ratio for CEMS, ^{57}Fe enriched chips (95.7%, 3 pieces, about 6.5mm×6.5mm×0.6mmt for each piece) were placed on a pure Fe disk target (99.9%, 55mmϕ×2mmt) when γ'-Fe_4N films were deposited.

Samples were fabricated in the following steps A, B and C. In steps A and B, we sought an optimum deposition condition for a γ'-Fe_4N single phase on silica glass by changing N_2 flow rates and substrate temperatures. Only the Fe disk was used as a target in step A, and the dummy chips were added in step B. Finally in step C, the ^{57}Fe enriched chips were placed on the disk instead of the dummy chips and ^{57}Fe enriched γ'-Fe_4N films were deposited on silica glass, MgO(001), MgO(111), $SrTiO_3$(001) and $SrTiO_3$(111) substrates by the optimum condition derived in step B. The pressure and flow rate of Ar gas were kept at 0.2Pa and 10.0sccm, respectively. The RF power applied to the target was 100W. The thickness of the films was about 2300Å.

Crystalline structure of the films was investigated by X-ray diffraction (XRD) with Cu-Kα radiation. Surface morphology of the films was observed by scanning electron microscopy (SEM). Magnetic properties of the films were investigated by measuring the magnetic moment versus magnetic field (M-H) hysteresis curves by vibrating sample magnetometer (VSM). The hyperfine structure of the films was examined by CEMS with ^{57}Co(Rh) source. The velocity was calibrated using α-Fe. All of these measurements were performed at room temperature.

3. RESULTS AND DISCUSSION

3.1 Growth condition

The XRD patterns of iron nitrides deposited on silica glass in step A and B are shown in Fig.1. In step A, γ'-Fe_4N single phase is successfully grown at the temperature of 600K and the flow rate of 1.0sccm (Fig. 1(a)). However, α-Fe is included in the film fabricated in step B at the optimum condition obtained in step A (Fig. 1(b-1)). The increase in surface area of the target led to the increase in sputter rate. So the N_2 flow rates are set at 1.1sccm and the substrate temperatures are gradually changed from 600K to 800K. A γ'-Fe_4N film with small, constant amount of ε-Fe_3N was fabricated up to 700K (Fig.1(b-2)). The ε phase was decreased at 750K and disappeared at 800K (Fig.1(b-3)).

The peak intensity of γ'-Fe_4N films fabricated in step A and B is different from each other. The strong (200) and (111) peaks are seen in Fig.1(a), while the relative peak intensity of each peak in Fig.1(b-3) becomes similar to those of bulk samples. This is due to thermal fluctuation.

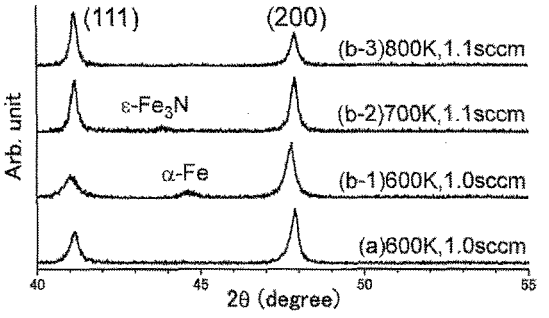

Fig.1: XRD patterns of iron nitride films deposited in step A and B.

The films are also observed by means of SEM. Both films consist of crystallites that are about 100 nm in diameter. The crystallites grown in step A have sharp edges and are close-packed. By contrast, those grown in step B are round and have gaps between each other. With such morphology, the γ'-Fe_4N film deposited in step B is easier to be oxidized.

3.2 Structure and surface morphology of γ'-Fe_4N films

Fig.2 shows the XRD patterns and SEM images of γ'-Fe_4N films grown on silica glass, MgO(001) and MgO(111) at the optimum condition found in step B (γ'/glass, γ'/MgO(001) and γ'/MgO(111), respectively). γ'/MgO(001) and γ'/MgO(111) are highly oriented and have the same orientation as their substrates. Both films, especially γ'/MgO(001), have very large grains. The crystallites as can be seen in γ'/glass and straight cracks are contained in γ'/MgO(111), but are not contained in γ'/MgO(001). Highly oriented γ'-Fe_4N films are also grown on $SrTiO_3$(001) and $SrTiO_3$(111) at the same condition (γ'/STO(001) and γ'/STO(111), respectively).

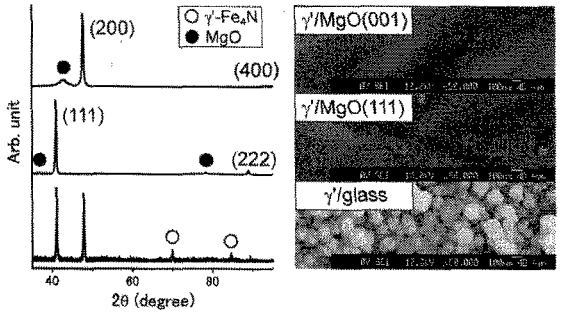

Fig.2: XRD patterns and SEM images of γ'-Fe_4N films on glass and MgO substrates.

Table I: Lattice parameters of γ'-Fe_4N films, bulk γ'-Fe_4N and MgO.

	d_{001} (Å)	d_{111} (Å)	d_{100} (Å)	α (deg.)
γ'/glass	3.804	2.198	3.791	89.82
γ'/MgO	3.815	2.201	3.785	89.74
γ'/STO	3.811	2.198	3.787	89.80
bulk γ'-Fe_4N	3.795	2.191	-	-
MgO	4.211	2.432	-	-
$SrTiO_3$	3.905	2.253	-	-

Table II: Difference in interplanar spacings between γ'-Fe_4N films on single crystals, bulk γ'-Fe_4N and substrates.

Substrate		MgO		$SrTiO_3$	
Form of γ'-Fe_4N		film	bulk	film	bulk
d (Å)	d_{001}	3.815	3.795	3.811	3.795
	d_{111}	2.201	2.191	2.198	2.191
d_{film}/d_{bulk}	d_{001}	1.005	-	1.004	-
	d_{111}	1.005		1.003	
$d_{substrate}/d_{\gamma'}$	d_{001}	1.104	1.110	1.025	1.029
	d_{111}	1.105		1.025	

The lattice parameters of γ'-Fe_4N films are shown in Table I. The out-of-plane interplanar spacings of the films d_{001} and d_{111} are derived from XRD patterns. The in-plane interplanar spacing d_{100} for tetragonally packed (001) planes and the angle between edges of an unit cell α for rhombohedrally packed (111) planes are calculated on the assumption that the volume and the length of an edge of a unit cell are the same as bulk, respectively. All the films are nearly cubic. However, their out-of-plane interplanar spacings d_{001} and d_{111} are larger than those of bulk, and γ'/MgO and γ'/STO have larger d_{001} and d_{111} than γ'/glass.

The difference in interplanar spacings between the films on single crystals, bulk γ'-Fe_4N and substrates are listed in Table II. The ratio between interplanar spacings of γ'-Fe_4N and the substrates are 1.110 and 1.029, that is to say, 11 and 41 γ'-Fe_4N unit cells correspond to 10 MgO and 40 $SrTiO_3$ unit cells, respectively. The 11 and 41 bulk γ'-Fe_4N unit cells are slightly smaller than corresponding substrate unit cells. The lattice of the films are expanded about 0.3-0.5% than bulk. This lattice expansion makes the ratio between interplanar spacings of γ'-Fe_4N and the substrates lower. Thus, the lattice mismatch between γ'-Fe_4N films and their substrates is remarkably reduced by the distortion in γ'-Fe_4N films.

3.3 Magnetic properties of γ'-Fe_4N films

The in-plane and out-of-plane M-H curves of γ'-Fe_4N films on glass and MgO substrates are shown in Fig.3. The values of saturation magnetization M_S and coercive force H_C for each film are listed in Table III. The effects of demagnetization field are not taken into consideration. All the films have smaller M_S than that of bulk.

Table III: Magnetic properties of γ'-Fe_4N films.

	in-plane		out-of-plane	
	M_S (emu/g)	H_C (Oe)	M_S (emu/g)	H_C (Oe)
γ'/glass	151	92	128	147
γ'/MgO(001)	166	35	129	77
γ'/MgO(111)	160	46	154	42

Two γ'/MgO films are sharply magnetized at low field when in-plane magnetic field is applied. At that time, γ'/MgO(001) has the smallest H_C and the largest M_S. The values of in-plane and out-of-plane H_C in γ'/MgO(111) are almost equivalent. γ'/glass has the largest H_C in both in-plane and out-of-plane M-H curves.

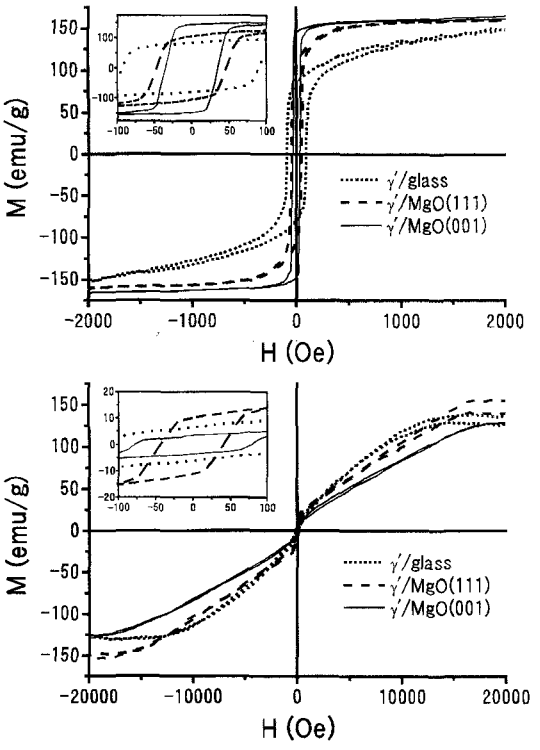

Fig.3: In-plane and out-of-plane M-H curves of γ'-Fe_4N films on glass and MgO substrates. The insets show the area around zero field.

These results are due to the morphology of the films. Spins are easily arranged in highly oriented films with large grains like in the cases of γ'/MgO. The behavior of magnetization of γ'/MgO depends on their crystalline orientation. In contrast, the randomly oriented crystallites in γ'/glass make domain walls hard to move.

3.4 Hyperfine structure of γ'-Fe_4N films

The CEMS spectra and hyperfine parameters of γ'-Fe_4N films are shown in Fig.4 and Table IV, respectively. Each spectrum is composed of three sextets

Table IV: Hyperfine parameters of γ'-Fe_4N films.

		HF (kOe)	QS (mm/s)	IS (mm/s)	RA (%)
γ'/glass	FeI	339.07	0.01	0.12	25
	FeIIA	215.85	0.03	0.25	50
	FeIIB	216.03	- 0.07	0.05	25
γ'/MgO (001)	FeI	336.81	0.00	0.12	25
	FeIIA	216.33	0.19	0.19	50
	FeIIB	214.60	- 0.38	0.18	25
γ'/MgO (111)	FeI	334.34	0.01	0.11	25
	FeIIA	214.34	0.10	0.20	50
	FeIIB	214.29	- 0.20	0.16	25
γ'/STO (001)	FeI	336.30	0.00	0.12	25
	FeIIA	215.70	0.21	0.19	50
	FeIIB	214.87	- 0.42	0.18	25
γ'/STO (111)	FeI	335.14	0.01	0.12	25
	FeIIA	211.45	0.16	0.21	50
	FeIIB	209.97	- 0.32	0.14	25

which indicate ferromagnetic Fe sites in γ'-Fe_4N.

The intensity of the peaks around ±2mm/s varies according to the substrates. In contrast, no substrate dependence is seen in hyperfine parameters. It is well known that the intensity ratio of three sub-doublets constituting one sextet depends on θ_R, the angle between sample magnetization and incident γ-ray [7]. The relationship between θ_S, the angle of sample magnetization to the substrate surface (θ_S=90°-θ_R), and intensity of sub-doublets $I_{(i,j)}$ are given by:

$$I_{(1,6)} : I_{(2,5)} : I_{(3,4)} = 3 : \frac{4\cos^2\theta_S}{1+\sin^2\theta_S} : 1 .$$

The sample magnetization is normal to the substrate surface when $I_{(2,5)}/I_{(3,4)}$ equals to zero, and if $I_{(2,5)}/I_{(3,4)}$ equals to four, the sample magnetizes completely in-plane. From the easy axis of magnetization, it can be expected that the angle θ_S for γ'-Fe_4N(001) and γ'-Fe_4N(111) would be 0° and 35.26°, respectively.

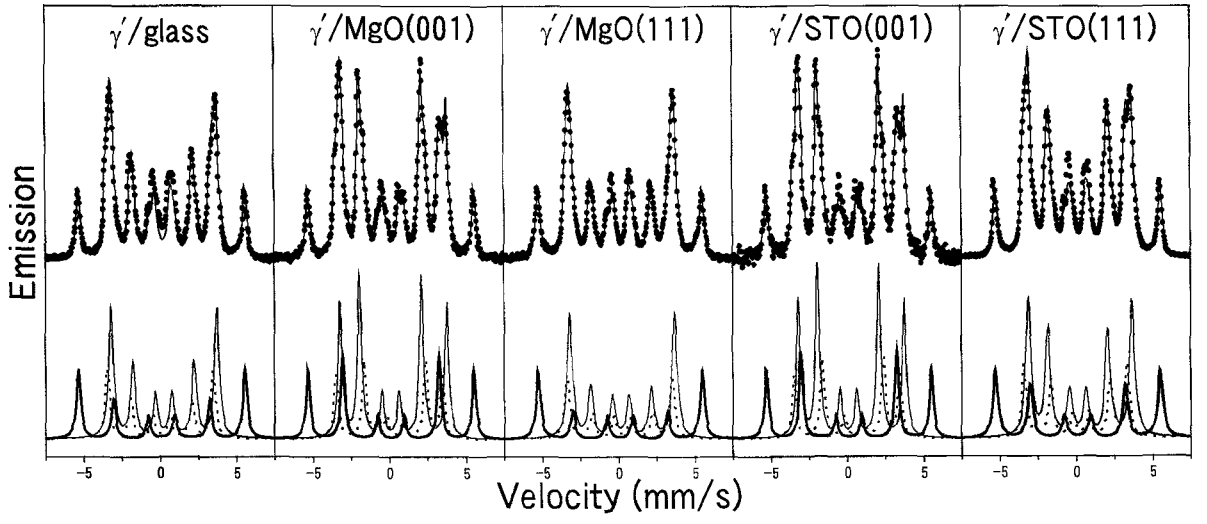

Fig.4: CEMS spectra of γ'-Fe_4N films. The lower spectra indicate Fe atoms at edge site FeI (thick solid line), fcc sites FeIIA (thin solid line) and FeIIB (dotted line).

Table V: Angles of magnetization of γ'-Fe_4N films to the substrate surface derived from relative intensity of sub-doublets in CEMS spectra.

	$I_{(2,5)}/I_{(3,4)}$		θ_S (deg.)	
	(001)	(111)	(001)	(111)
γ'/glass	1.70		39.40	
γ'/MgO	3.59	1.22	13.41	46.80
γ'/STO	3.74	2.34	10.53	30.72
Expected	4.00	2.00	0.00	35.26

The values of θ_S for each film derived from Fig.4 are shown in table V. The relative intensity of the (2,5) sub-doublet of γ'/glass is about two, so the film magnetizes at random. For the (001)-oriented films and γ'/STO(001), θ_S are larger than expected value. In contrast, γ'/STO(111) has smaller θ_S than expected, as is reasonable because films tend to magnetize in in-plane direction due to the effect of demagnetizing field [8].

Fig. 5 shows the relation between rates of lattice expansion and angles θ_S for the films. If the rate is larger than a certain value, the effect of lattice expansion overcomes that of demagnetizing field and the angle of magnetization becomes larger. So we concluded that the direction of magnetization of the films except for γ'/STO(111) is due to the large lattice expansion in the film.

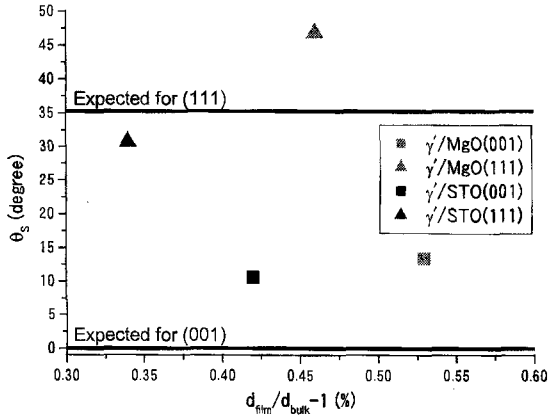

Fig.5: Relationship between lattice expansion of the films and angles of magnetization.

4. CONCLUSION

Highly oriented γ'-Fe_4N films were successfully grown on MgO(001), MgO(111), $SrTiO_3$(001) and $SrTiO_3$(111) substrates. The interplanar spacings of γ'-Fe_4N films on MgO and $SrTiO_3$ are enlarged in order to reduce the lattice mismatch between the films and substrates. The behavior of magnetization in the films observed by VSM and CEMS depends on the structure and crystalline orientation of the films. The (111)-oriented films show an out-of-plane magnetic anisotropy, and the films on MgO(001), MgO(111) and $SrTiO_3$(001) magnetize at larger angle to the substrates than expected due to the large lattice expansion.

ACKNOWLEDGMENTS

This work is supported by the Grant-in-Aid for Specially Promoted Research from the Ministry of Education, Culture, Sports, Science and Technology (12CE2004 Control of Electrons by Quantum Dot Structures and Its Application to Advanced Electronics).

References

[1] (For example) C. Chang, J. M. Sivertsen and J. H. Judy, *IEEE Trans. Magn.*, **MAG-23**, 3636-38 (1987).
[2] E. Kita and A. Tasaki, *Kotai Butsuri*, **11**, 721-27 (1984).
[3] J. C. Wood, Jr. and A. J. Nozik, *Phys. Rev. B*, **4**, 2224-28 (1971).
[4] D. M. Borsa, S. Grachev and D. O. Boerma, *NATO Science Series, II*, **41**, 445-48 (2001).
[5] R. Loloee, K. R. Nikolaev and W. P. Pratt, Jr., *Appl. Phys. Lett.*, **82**, 3281-83 (2003).
[6] D. M. Borsa, S. Grachev and D. O. Boerma, *IEEE Trans. Magn.*, **38**, 2709-11 (2002).
[7] E. Fujita, "Mössbauer bunko nyumon", Agne Gijutsu Center, Tokyo (1999) pp. 36.
[8] Y. Shiraki and S. Yoshida, "Hakumaku Kougaku", Maruzen, Tokyo (2003) pp. 215.

(Received October 10, 2003; Accepted March 20, 2004)